



**HAL**  
open science

## **LysoPE mediated by respiratory microorganism Aeromicrobium camelliae alleviates H9N2 challenge in mice**

Qingsong Yan, Junhong Xing, Ruonan Zou, Mingjie Sun, Boshi Zou, Yingjie Wang, Tianming Niu, Tong Yu, Haibin Huang, Wentao Yang, et al.

► **To cite this version:**

Qingsong Yan, Junhong Xing, Ruonan Zou, Mingjie Sun, Boshi Zou, et al.. LysoPE mediated by respiratory microorganism *Aeromicrobium camelliae* alleviates H9N2 challenge in mice. *Veterinary Research*, 2024, 55 (1), pp.136. 10.1186/s13567-024-01391-x . hal-04734360

**HAL Id: hal-04734360**

**<https://hal.science/hal-04734360v1>**

Submitted on 14 Oct 2024

**HAL** is a multi-disciplinary open access archive for the deposit and dissemination of scientific research documents, whether they are published or not. The documents may come from teaching and research institutions in France or abroad, or from public or private research centers.


L'archive ouverte pluridisciplinaire **HAL**, est destinée au dépôt et à la diffusion de documents scientifiques de niveau recherche, publiés ou non, émanant des établissements d'enseignement et de recherche français ou étrangers, des laboratoires publics ou privés.

RESEARCH ARTICLE

Open Access



# LysoPE mediated by respiratory microorganism *Aeromicrobium camelliae* alleviates H9N2 challenge in mice

Qingsong Yan<sup>1†</sup>, Junhong Xing<sup>1†</sup>, Ruonan Zou<sup>1</sup>, Mingjie Sun<sup>1</sup>, Boshi Zou<sup>1</sup>, Yingjie Wang<sup>1</sup>, Tianming Niu<sup>1</sup>, Tong Yu<sup>1</sup>, Haibin Huang<sup>1</sup>, Wentao Yang<sup>1</sup>, Chunwei Shi<sup>1\*</sup>, Guilian Yang<sup>1\*</sup> and Chunfeng Wang<sup>1\*</sup>

## Abstract

Influenza remains a severe respiratory illness that poses significant global health threats. Recent studies have identified distinct microbial communities within the respiratory tract, from nostrils to alveoli. This research explores specific anti-influenza respiratory microbes using a mouse model supported by 16S rDNA sequencing and untargeted metabolomics. The study found that transferring respiratory microbes from mice that survived H9N2 influenza to antibiotic-treated mice enhanced infection resistance. Notably, the levels of *Aeromicrobium* were significantly higher in the surviving mice. Mice pre-treated with antibiotics and then inoculated with *Aeromicrobium camelliae* showed reduced infection severity, as evidenced by decreased weight loss, higher survival rates, and lower lung viral titres. Metabolomic analysis revealed elevated LysoPE (16:0) levels in mildly infected mice. In vivo and in vitro experiments indicated that LysoPE (16:0) suppresses inducible nitric oxide synthase (iNOS) and cyclooxygenase-2 (COX2) expression, enhancing anti-influenza defences. Our findings suggest that *Aeromicrobium camelliae* could serve as a potential agent for influenza prevention and a prognostic marker for influenza outcomes.

**Keywords** Influenza, respiratory microbiota, *Aeromicrobium camelliae*, LysoPE (16:0)

## Introduction

Influenza is an acute viral respiratory disease that poses a significant threat to human and animal health, with seasonal outbreaks impacting thousands of both each year.

Influenza viruses are classified according to the antigenic properties of their surface glycoproteins, with four main types identified so far [1]. Among these, the influenza A virus is recognised as an avian influenza strain [2]. As members of the *Orthomyxoviridae* family, these viruses have a segmented negative-sense RNA genome that encodes ten core proteins and a varying number of accessory proteins [3, 4]. They are further divided into 18 HA and 11 NA subtypes based on their surface glycoproteins: HA and NA [5]. Certain subtypes can cause serious infectious diseases in animals, resulting in significant economic losses for the poultry industry. Notably, China has experienced a clear increase in avian influenza cases in recent years [6].

Moreover, the H9N2 subtype, first isolated from turkeys in Wisconsin, USA, in 1966, has since spread globally [7–10]. The virus is common in various avian species

Handling editor: Marie Galloway.

<sup>†</sup>Qingsong Yan and Junhong Xing have contributed equally to this work.

\*Correspondence:

Chunwei Shi  
shichunwei@jlau.edu.cn  
Guilian Yang  
yangguilian@jlau.edu.cn  
Chunfeng Wang  
wangchunfeng@jlau.edu.cn

<sup>1</sup> College of Veterinary Medicine, Jilin Provincial Engineering Research Center of Animal Probiotics, Jilin Provincial Key Laboratory of Animal Microecology and Healthy Breeding, Engineering Research Center of Microecological Vaccines (Drugs) for Major Animal Diseases, Ministry of Education, Jilin Agricultural University, Changchun 130118, China



© The Author(s) 2024. **Open Access** This article is licensed under a Creative Commons Attribution 4.0 International License, which permits use, sharing, adaptation, distribution and reproduction in any medium or format, as long as you give appropriate credit to the original author(s) and the source, provide a link to the Creative Commons licence, and indicate if changes were made. The images or other third party material in this article are included in the article's Creative Commons licence, unless indicated otherwise in a credit line to the material. If material is not included in the article's Creative Commons licence and your intended use is not permitted by statutory regulation or exceeds the permitted use, you will need to obtain permission directly from the copyright holder. To view a copy of this licence, visit <http://creativecommons.org/licenses/by/4.0/>. The Creative Commons Public Domain Dedication waiver (<http://creativecommons.org/publicdomain/zero/1.0/>) applies to the data made available in this article, unless otherwise stated in a credit line to the data.

worldwide, mainly chickens and ducks, but it can also infect humans and other mammals, making it a zoonotic disease [11]. Certain strains of H9N2 have evolved to bind receptors necessary for human infection, leading to mild respiratory illnesses and posing a significant health risk [12]. Avian Influenza Viruses (AIV) are divided into two categories based on their pathogenicity in chickens and molecular markers in HA proteins: highly pathogenic avian influenza viruses (HPAIV) and low pathogenic avian influenza viruses (LPAIV), known for their high and low pathogenicity, respectively [13]. Despite the H9N2 strain being classified as an LPAIV, it can still interact with other pathogens, thus reducing poultry performance, causing severe clinical symptoms, and increasing mortality rates [14–17]. Moreover, H9N2 AIV has been isolated from various mammals and can transfer genetic material to other influenza subtypes such as H5, H1, or H7. This ability to transfer can potentially create new viruses with increased pathogenicity [18–20]. Therefore, the widespread presence of the H9N2 virus across species could lead to a new influenza pandemic, threatening human and animal health [21, 22].

Scientific advancements have led to the identification of distinct microbial communities within the gastrointestinal tract that play a crucial role in maintaining host health [23, 24]. Known as ‘next-generation probiotics’, these beneficial commensal microorganisms are increasingly used to restore a healthy balance within the gastrointestinal environment [25]. Bacteria such as *Clostridium butyricum*, *Bacillus salivarius*, and *Akkermansia muciphila* have been shown to regulate immune responses in this tract [26–28]. The respiratory system also contains a diverse microbiota, with variations in types and quantities across different sections [29]. Numerous studies have demonstrated the microbiota’s role in enhancing host immunity, improving nutrient absorption, and strengthening the intestinal barrier [30, 31]. Specific microbial communities have recently been found throughout the respiratory tract, from the nostrils to the alveoli [32]. Changes in the composition or functionality of the respiratory microbiota can decrease the population of beneficial bacteria, compromising the respiratory system’s ability to defend against pathogens [33]. Although research on respiratory microbiota is not as extensive as it is for gastrointestinal microbiota, some studies have highlighted the beneficial impact specific bacteria can have on respiratory health, which has opened avenues for exploring and identifying novel respiratory ‘next-generation probiotics’ [34].

Microorganisms play a crucial role in maintaining host health, but they can also promote disease through microbiota dysbiosis. In addition to their digestive functions, these microorganisms produce various

vitamins and benefit the host by producing short-chain fatty acids (SCFAs) such as butyrate, propionate, and acetate [35]. Metabolites are classified into three main types: (1) those produced by the intestinal microbiota from dietary components, such as vitamin K; (2) those secreted by host cells and modified by the gut microbiota, like secondary bile acids; and (3) those formed through the intestinal microbiota’s anaerobic fermentation, exemplified by SCFAs [36–38]. The microbiota and its metabolites are critical in regulating host physiology and pathophysiology, influencing a wide range of metabolic, inflammatory, and even behavioural processes [39, 40]. Studies have shown that microbial metabolites can modulate the host’s immune responses [41, 42].

LysoPE is a lysophospholipid produced by phosphatidylethanolamine (PE) deacylation during hydrolysis by phospholipase A1/A2 [43]. It has been found to affect lipid accumulation and metabolism in human liver-derived cell lines [44]. LysoPE also acts as a neurotrophic activator through the mitogen-activated protein kinase signalling pathway in pheochromocytoma cells [45]. Recent research has demonstrated that LysoPE not only enhances neurite outgrowth but also protects cultured cortical neurons against glutamate toxicity. Furthermore, it inhibits lipopolysaccharide-induced polarisation of M1 macrophages in murine peritoneal macrophages [46–48].

Thus, investigating the protective effects of respiratory flora and their metabolites on host organisms is essential for developing novel anti-influenza agents.

## Materials and methods

### Bacteria, viruses, and animals

*Aeromicrobium camelliae* was obtained from the China Microbial Strain Collection and Management Centre, catalogued under strain number JCM 30952, and cultured aerobically at 37 °C for 24 h in a Lysogeny Broth (LB) liquid medium.

J774A.1 and MDCK cells are maintained in our laboratory.

Our laboratory also preserves the H9N2 strain [49]. The virus’s titre was determined using the half-maximal infective dose (H9N210<sup>6.5</sup>EID<sub>50</sub>) in chicken embryos. Specific-pathogen-free (SPF) six-week-old C57BL/6 female mice were sourced from Changchun Yis Experimental Animal Technology Co. The mice were housed with unlimited access to water and food at the SPF Animal Farming Center. All animal-related procedures were performed in strict compliance with the guidelines of the Animal Management and Ethics Committee of Jilin Agricultural University (JLAU20200704001).

### Statistical analysis

Data were analysed using GraphPad Prism 8.0 software. Pairwise comparisons were conducted with the Student's *t*-test, and values are presented as mean  $\pm$  SD. \**p* < 0.05, \*\**p* < 0.01, \*\*\**p* < 0.001.

### Experimental design and sample collection

The experimental framework was divided into four groups: Experiment A for establishing the H9N2 mouse model, Experiment B for inoculating mice with respiratory microorganisms, Experiment C for microbial terpene administration, and Experiment D for LysoPE (16:0) administration.

**Experiment A:** Six-week-old female C57BL/6 mice were divided into two groups: the infected group (*n* = 20) and the control group (*n* = 5; NC). On day 0, mice were intranasally inoculated with H9N2 (20  $\mu$ L/animal). Post-inoculation, we conducted daily monitoring for 15 days (from day 0 to day 14) to assess the weight and survival of the mice. Concurrently, lung tissue, blood, and bronchoalveolar lavage fluid were collected from the subjects on day five post-inoculation. Part of the lavage fluid was frozen at -80 °C for future 16S sequencing and non-targeted metabolomics analysis. The remainder of the lavage fluid was centrifuged at 6000  $\times$  *g* for 15 min, suspended in 10% glycerol, and stored at -80 °C. Lung specimens were fixed in 4% formaldehyde, embedded in paraffin, and subjected to haematoxylin and eosin (H&E) staining for histopathological evaluation and immunohistochemistry. Based on post-inoculation, lung viral loads and body weight trajectories, mice were classified into severe (S) and mild (M) subsets.

**Experiment B:** The collected bronchoalveolar lavage fluid was centrifuged. Glycerin was replaced by phosphate-buffered saline (PBS) and stained with methylene blue to quantify live microorganisms. Resuspension in PBS at 1  $\times$  10<sup>6</sup> CFU/40  $\mu$ L was prepared for subsequent use [50]. Twenty antibiotic (ATB) pre-treated mice were randomly divided into four groups (*n* = 5/group). These groups were Group M, the nasal toxicity group with irrigation solution (Donor M + H9N2), Group S, the nasal toxicity group with irrigation solution (Donor S + H9N2), the PBS-inoculated group (PBS + H9N2), and the control group (NC). Mice in the Donor M and Donor S groups received a one-day nasal drip, while those in the PBS + H9N2 group received an equivalent volume of PBS. One day after intranasal inoculation with H9N2 (20  $\mu$ L/vessel), mice were monitored daily for body weight and survival for 15 days (post-infection day 0 to day 14). A concurrent experiment replicated sample collection as outlined in Experiment A.

**Experiment C:** Before the virulence test, *Aeromicrobium* was aerobically incubated for 24 h, centrifuged at 4000  $\times$  *g* for 4 min at 4 °C, washed three times with sterile PBS (pH = 7.4), and resuspended in PBS at 1  $\times$  10<sup>8</sup> CFU/40  $\mu$ L for subsequent application. Fifteen ATB pre-treated mice were randomly assigned to three groups (*n* = 5/group). These were the control (NC), *Aeromicrobium*-inoculated group (Ae + H9N2), and PBS-inoculated group (PBS + H9N2). Mice in the Ae + H9N2 group received *Aeromicrobium camelliae* via nasal administration for five days, while those in the PBS + H9N2 group received an equivalent volume of PBS. Following this, both groups, excluding the control, were intranasally inoculated with H9N2 (20  $\mu$ L per mouse), with subsequent monitoring of survival and body weights for 14 days post-infection. A parallel study was conducted to replicate sample collection as per Experiment A.

**Experiment D:** To assess the anti-influenza efficacy of LysoPE (LysoPE (16:0), purchased from Sigma-Aldrich), 15 ATB pre-treated mice were randomly divided into three groups (*n* = 5/group). These included the control group (NC), metabolite repletion attack group (LysoPE + H9N2), and Vehicle attack group (Vehicle + H9N2). Mice in the LysoPE + H9N2 group were given LysoPE (1 mg/kg; 20  $\mu$ L) (1% DMSO dissolved in PBS) via nasal drip for five days. Mice in the Vehicle group received the same volume of PBS via nasal drip. Five days later, the remaining groups, excluding the control, were intranasally challenged with H9N2 (20  $\mu$ L per mouse), and their survival and body weights were tracked for 14 days post-infection. Concurrently, a replicated study was undertaken for sample collection, as detailed in Experiment A.

### J774A.1 cell inflammation model establishment

J774A.1 cells were cultured in Dulbecco's Modified Eagle Medium (DMEM) (1% double antibody, 5% serum) and inoculated onto 12-well plates (2  $\times$  10<sup>5</sup> cells/well) for 24 h. Cells were treated with lipopolysaccharide (LPS) at concentrations of 100, 500, and 1000 ng/mL for 6 h. RNA was extracted from the cells, reverse transcribed, and quantified via qRT-PCR.

### LysoPE inhibition of J774A.1 cell inflammatory response model

J774A.1 cells were cultured in DMEM medium (1% double antibody, 5% serum) and inoculated onto 12-well plates (2  $\times$  10<sup>5</sup> cells/well) for 24 h. Cells were pre-treated with LysoPE at concentrations of 1  $\mu$ M, 10  $\mu$ M, and 50  $\mu$ M for 24 h, followed by 6-h stimulation with 1  $\mu$ g/mL LPS. RNA was subsequently extracted, reverse transcribed, and quantified using qRT-PCR, with further analysis through protein blotting.

### Collection of mouse alveolar macrophages

Alveolar macrophages (AMs) were isolated via BALF (bronchoalveolar lavage fluid). Following the euthanasia of the mice, the lungs were lavaged with Hanks' balanced salt solution (HBSS). This process involved the slow injection and withdrawal of 2 mL of warm (37 °C) Ca<sup>2+</sup>/Mg<sup>2+</sup>-free HBSS (pH 7.4) with EDTA (0.6 mM), which was performed eight times [51]. The lavage fluid was collected and centrifuged (400×g, 10 min, 4 °C), and the cells were prepared for subsequent applications.

### Antibiotic-treated mice

Following the procedures used in previous studies, the mice received one week of intranasal administration of 50 µL ddH<sub>2</sub>O containing ampicillin (1 mg/mL), vancomycin (0.5 mg/mL), metronidazole (1 mg/mL), and neomycin (1 mg/mL) to eradicate respiratory microbiota [52].

### 16srDNA sequencing

The hexadecyltrimethylammonium bromide (CTAB) method was used to extract the total microbiome DNA from various sample origins. We assessed the DNA quality by running it through agarose gel electrophoresis and using a UV spectrophotometer for quantification. To delineate the taxonomic composition of the mouse respiratory microbiome, the V3-V4 region of the 16 S rDNA gene was targeted for sequencing with commonly used primers (F: 5'-CCTACGGGNGGCWGCAG-3'; R: 5'-GACTACHVGGGTATCTAATCC-3'). Amplification reactions were prepared using 50 ng of template DNA in a total volume of 25 µL. PCR conditions included an initial denaturation at 98 °C for 30 s, followed by 35 cycles of 10 s at 98 °C, 30 s at 54 °C, and 45 s at 72 °C, with a final extension of 10 min at 72 °C.

Following purification, we evaluated the PCR products using the Agilent 2100 Bioanalyzer (Agilent, USA) in conjunction with Illumina library quantification kits (Kapa Biosciences, Woburn, MA, USA). Acceptable library concentrations were established at a minimum of 2 nM. Qualifying libraries, ensuring non-repetitive index sequences, were diluted based on the required sequencing depth, denatured to single strands with NaOH, and prepared for sequencing. A 2×250 bp paired-end sequencing protocol was executed on the NovaSeq 6000 platform.

Diversity analysis was divided into alpha and beta diversity assessments based on the procured Amplicon Sequence Variant (ASV) sequences and corresponding abundance tables. Alpha diversity within the microbial communities was quantified using six indices: Observed\_species, Shannon, Simpson, Chao1, Goods\_coverage, and Pielou\_e. Beta diversity was assessed by calculating four

distances to assess diversity between habitats (between samples/groups), using six main analyses (Weighted\_unifrac, Unweighted\_unifrac, Jaccard, Bray\_curtis).

**Species Annotation:** Using the SILVA database, species were identified based on the ASV sequences and further annotated with the NT-16S database. Subsequently, the abundance of each species within individual samples was enumerated based on the ASV abundance table.

**Variance and Subsequent Analysis:** The discrepancies between comparative groups were analysed based on the species abundance data retrieved. The selection of an appropriate statistical method was contingent upon the sample specifics. In this study, the Kruskal–Wallis test was employed to distinguish the differences among multiple groups, each comprising biological replicates of the samples ( $p < 0.05$ ).

### Non-targeted metabolomics analysis

The acquired liquid samples were initially thawed on ice, and 20 µL of each sample was extracted with 120 µL of pre-cooled 50% methanol. The samples were vortexed for 1 min, incubated at room temperature for 10 min, and stored overnight at -20 °C. Following centrifugation at 4000 g for 20 min, the supernatant was transferred to a fresh 96-well plate and preserved at -80 °C prior to LC–MS analysis. Concurrently, quality control (QC) samples were prepared by combining 10 µL from each extract. After sample preparation, the extracts underwent systematic analysis. Initially, the raw mass spectral data were converted into an interpretable format using Proteowizard msConvert software, converting to mzXML. XCMS software facilitated peak extraction, which was then subjected to QC. CAMERA was used for compound annotation and preliminary identification via metaX software. This identification included Level 1 mass spectrometry information, and Level 2 mass spectrometry data correlated with an in-house standards database. The putative identifiers were further annotated using databases such as HMDB and KEGG, which elucidate the metabolites' physicochemical properties and biological functions. Differential metabolites were quantified and screened using metaX software.

### Analysis of cytokine concentrations

The blood samples were allowed to clot overnight at 4 °C, followed by centrifugation to obtain the serum (1000 rpm, 4 °C, 5 min). The lung tissues were homogenised in PBS at a 1 mL/0.1 g lung ratio, and the homogenate was clarified by centrifugation (3000 rpm, 4 °C, 5 min). Cytokine levels, specifically TNF- $\alpha$ , IL-1 $\beta$ , and IL-6, were assessed using ELISA kits according to the manufacturer's protocol. The absorbance was calculated at 450 nm with an enzyme-linked immunosorbent assay

reader, and cytokine concentrations were deduced from a standard curve.

### Virus titre detection

To determine the virus titre and obtain a serially diluted tenfold suspension of tissue homogenate, an equal weight of lung tissue was homogenised in DMEM. It was then titrated in 96-well culture plates of MDCK cells. The Reed-Muench method was adopted to calculate the titre, which was expressed as  $\log_{10}$ TCID<sub>50</sub>/g of lung tissue [53].

### Histological analysis

The mouse lung tissues were fixed in 4% formaldehyde, embedded in paraffin, and sectioned. Each sample comprised at least two tissue section (3  $\mu$ m). These sections were heated in an oven at 80 °C for 1 h, then cooled to room temperature. After the haematoxylin–eosin (H&E) staining, the sections were observed through an inverted fluorescence microscope (Leica Microsystems, Germany).

### Immunohistochemical analysis

The lung tissue was fixed in 4% formaldehyde, paraffin-embedded, and sectioned. Each sample contained at least two tissue sections of 3  $\mu$ m thickness. Sections were then baked at 80 °C for 2 h, dewaxed and immersed in antigen retrieval solution (1 $\times$ ; sodium citrate antigen repair solution 50 $\times$ , diluted with double distilled water). The solution was preheated to 95 °C–100 °C, and sections were heated for approximately 20 min at this temperature. After cooling, sections were rinsed twice with PBS for 5 min each. The tissue perimeters were circumscribed using a 0.3% Triton-100 pen, allowing for membrane permeabilisation. They were then incubated in darkness at room temperature for 60 min.

After discarding the liquid and blotting, sections were incubated with the diluted primary antibody (H9N2 monoclonal sheep anti-rabbit antibody purchased from SinoBiological; 1:1000 PBS dilution) overnight at 4 °C in the light. On the following day, the sections were washed three times with PBS for 5 min each. After blotting, sections were incubated with the secondary antibody (H9N2 secondary antibody sheep anti-rabbit purchased from Servicebio; 1:600 PBS dilution) and incubated for 1 h at room temperature. They were then washed twice with PBS for 5 min each. DAPI (1:1000 PBS dilution) was applied for 5 min, protected from light, followed by three PBS washes for another 5 min each. Sections were finally analysed using an inverted fluorescence microscope (Leica Microsystems, Germany).

### Quantitative real-time PCR

Using the TaKaRa MiniBEST Universal RNA Extraction Kit, total RNA was extracted from treated J774A.1 cells and mouse AMs. Complementary DNA (cDNA) was synthesised from approximately 2  $\mu$ g of total RNA using the SweScript All-in-One RT SuperMix for qPCR Synthesis Kit (Servicebio). The mRNA expression of TNF- $\alpha$ , IL-1 $\beta$ , IL-6, INOS and COX was analysed on a real-time fluorescent quantitative PCR assay system using the SYBR green premix kit (Servicebio). mRNA expression levels were calculated using the  $2^{-\Delta\Delta C_t}$  method and normalised to Glyceraldehyde-3-Phosphate Dehydrogenase (GAPDH). The primer sequences are as follows: mouse TNF- $\alpha$ , forward 5'-TTGTCTACTCCCAGGTTCTCT-3' reverse 5'-GAGGTTGACTTTCTCCTGGTATG-3'; mouse IL-6, forward 5'-CTGCAAGAG ACTTCCATCCAG-3', reverse 5'-AGTGGTATAGACAGGTCTGTTGG; mouse IL-1 $\beta$  forward 5'-AACCTGCTGGTGTGTGACGTT C-3', reverse 5'-CAGCACGAG GCTTTTTTGTG T-3'; mouse INOS forward 5'-GGAATCTTGAGCGA GTTGT-3', reverse 5'-CCTCTTGTCTTTGACCCA GTAG-3', mouse COX-2, forward 5'-CGGACTGGA TTCTATGGTGA-3', reverse 5'-CTTGAAGTGGGT CAGGATGTAG-3'; mouse GAPDH, forward 5'-AAC GTGTCAGTCGTGGACCTG-3', reverse 5'-AGT GGG TGTCGCTGTFGAAGT-3'.

### Protein blotting analysis

The cells were centrifuged in RIPA buffer (Beyotime) containing PMSF (Servicebio), totipotent nuclease (Servicebio), and phosphatase inhibitor (Servicebio) at 3500 rpm for 2 min to collect the cell supernatant. We used the BCA protein assay kit (Beyotime) to determine protein concentrations. The protein samples (10  $\mu$ g/lane) underwent separation via MOPS-PAGE and were then transferred to a polyvinylidene difluoride (PVDF) membrane. The membranes were blocked using rapid blocking solution (Beyotime) for 30 min at room temperature before overnight incubation with antibodies targeting INOS, COX-2, and GAPDH (Proteintech) at 4 °C. Thereafter, the membrane was exposed to the relevant horseradish peroxidase-linked secondary antibody (Servicebio) for 1 h at room temperature. Protein bands were then made visible using an enhanced chemiluminescence (ECL) system.

## Results

### C57bl/6 mice differentially targeted for H9N2 infection

The above processes found that mice infected with H9N2 exhibited different clinical symptoms. For example, all mice in Group S displayed pronounced signs of infection, including weight loss, anorexia, and a coarse coat

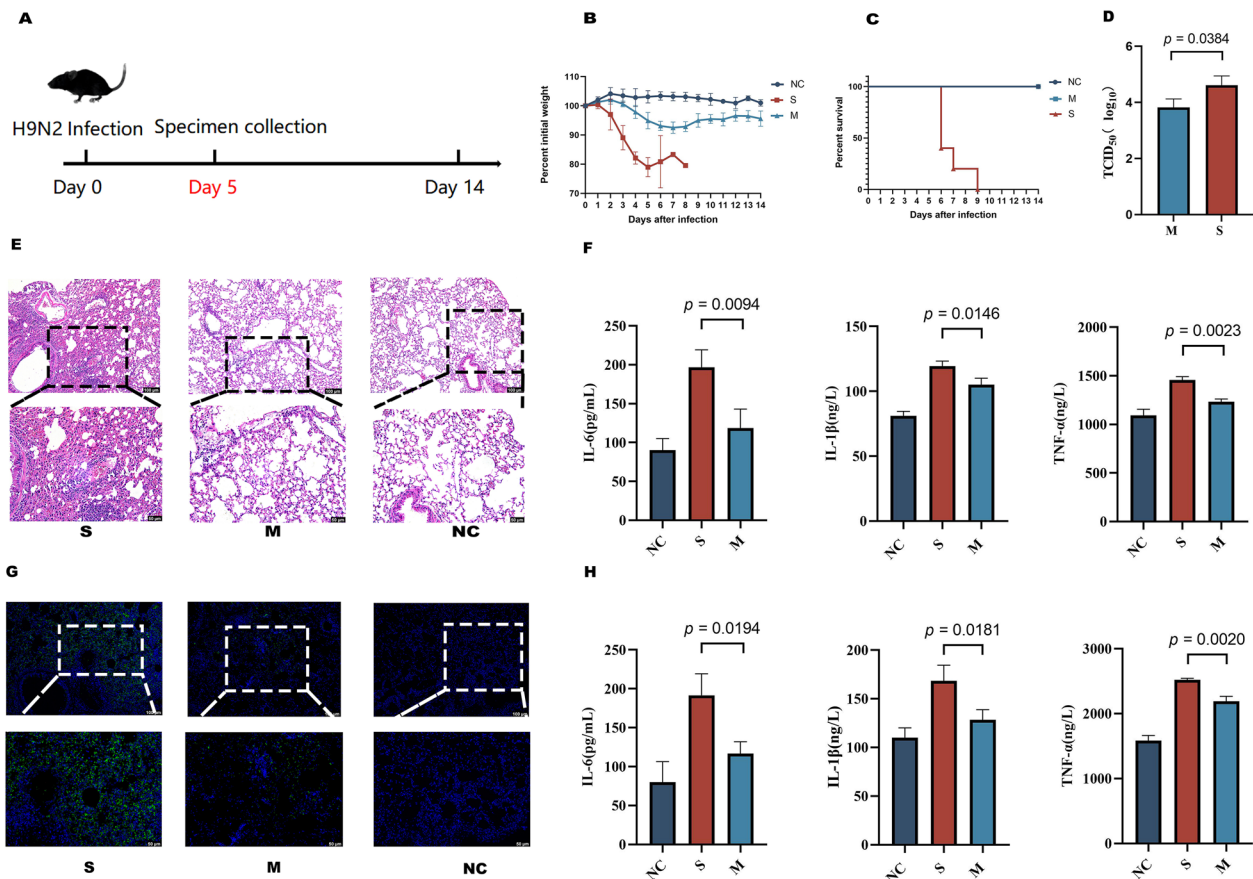


**Figure 1** Mice exhibit a heterogeneous response to influenza infection. **A** Experimental procedure. **B** Variability in body weight. **C** Survival rates. **D** Pulmonary virus load ( $\log_{10}$ TCID<sub>50/g</sub> of lung tissue). **E** H&E staining of mouse lung tissue. **F** Serum cytokine levels. **G** Immunohistochemical analysis of lung tissue. **H** Lung tissue cytokine levels. Data are presented as mean  $\pm$  SD. S: Severe infection group; M: Mild infection group.

(Figure 1B and C). All mice from the NC and M groups survived, with the NC group showing no evident signs of infection. Mice in Group M exhibited fewer signs of infection than those in Group S. The virus titre test results indicated that the pulmonary virus titre in Group M was significantly lower than in Group S (Figure 1D). The histopathological and immunohistochemical evaluations revealed that the M group had less severe lung lesions and a lower viral load than Group S (Figure 1E and G). The ELISA assay results showed higher levels of inflammatory cytokines TNF- $\alpha$ , IL-1 $\beta$ , and IL-6 in the lungs and serum of Group S compared to the other two groups (Figure 1F and H).

#### Transfer of respiratory microbiota in mice

We conducted respiratory microbiota transplants to determine if differential mouse responses to influenza infection correlated with variations in respiratory microbiota. We then evaluated the impact of respiratory microbiota transferred from mice in groups S and

M on viral infection in recipient mice (Figure 2A). The data showed that transferring respiratory microbiota from Group M mice to recipients on the fifth day after infection augmented their chances of survival.

Conversely, recipients that received respiratory microbiota from Group S displayed heightened infection rates (Figure 2B and C). The results of virus titre detection showed that the lung virus titre in the Donor M group was significantly lower than in the Donor S group (Figure 2D). Histopathological and immunohistochemical analyses revealed fewer lung pathologies and a reduced lung viral load in the Donor M group than in the Donor S group (Figure 2E and G). ELISA results indicated that cytokines TNF- $\alpha$ , IL-1 $\beta$ , and IL-6 levels were more pronounced in both serum and lungs of mice from the Donor S group than in the remaining groups (Figure 2F and H). These findings suggest that the respiratory microbiota in mice that survived the infection may contain specific respiratory microbes that provide protection against influenza.

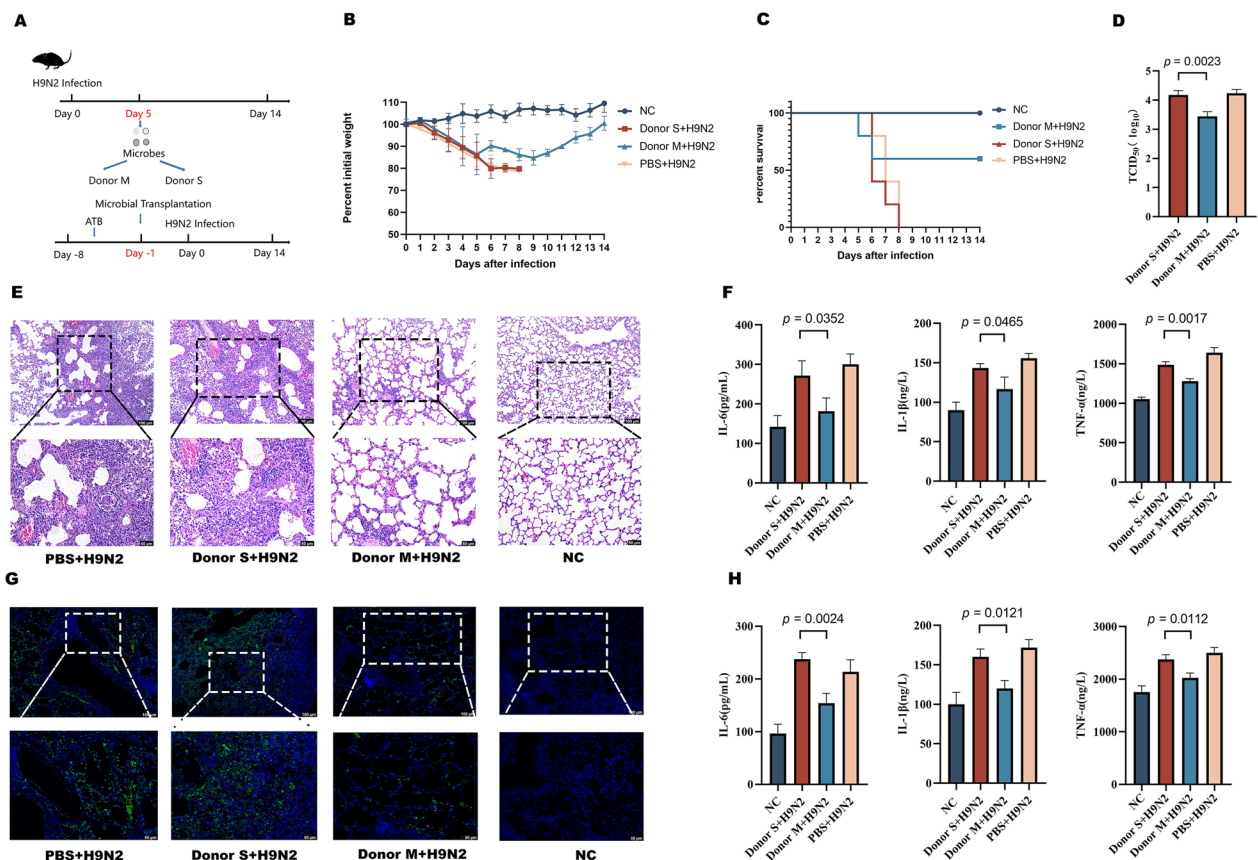


**Figure 2** Variability in response to influenza due to differences in respiratory microbiota in mice. **A** Experimental procedure. **B** Changes in body weight. **C** Survival rates. **D** Viral load in lungs ( $\log_{10}$ TCID<sub>50</sub>/g of tissue). **E** H&E staining of lungs. **F** Levels of cytokines in serum. **G** Immunohistochemical evaluations of the lungs. **H** Cytokine levels in lung tissues. Data are expressed as mean  $\pm$  SD. Donor M: transfer from mild infection group; Donor S: transfer from severe infection group.

### The respiratory microbiota exhibits distinctive characteristics depending on the severity of the influenza infection

To explore influenza-resistant respiratory microbes in mice that survived the infection, 16S rDNA sequencing was used to assess the respiratory microbiota of mice from the S, M, and NC groups on the fifth day of the study. The findings show that the species abundance table exposed marked variances in species count between the M and S groups (Figure 3A). Furthermore, the alpha diversity analysis results indicated that the NC group had the highest species count and greater diversity than the M and S groups. However, the M group maintained greater species count and diversity than the S group (Figure 3C). Both principal coordinate analysis (PCoA) and non-metric multidimensional scaling (NMDS) analyses pinpointed disparities in species composition between the M and S groups (Figure 3B).

Furthermore, when considering the phylum level, it was observed that the respiratory microorganisms' composition in all three groups predominantly

consisted of *Proteobacteria*, *Actinobacteria*, *Bacteroidota*, *Firmicutes*, and *Deinococcota*. Notably, the presence of *Proteobacteria* was significantly greater in the M and S groups than in the NC group. From the point of view of genera, *Pseudomonas* spp., *Ralstonia* spp., *Stenotrophomonas* spp., *Empedobacter* spp., and *Aeromicrobium* spp. dominated, and the abundance of *Pseudomonas* spp., was significantly higher in group S than that of group NC and group M. *Ralstonia* spp., *Stenotrophomonas* spp., *Empedobacter* spp., and *Aeromicrobium* spp. were more abundant in group M than that of group S (Figure 4B). The LEfSe variance analysis revealed that certain species, such as *Pseudomonas*, *Bacillus thuringiensis*, and *Agathobacter recti*, were particularly distinct in Group M. Meanwhile, in Group S, *Burkholderia*, *Ralstonia*, *Propionibacteriales*, and *Nocardioidaceae* were distinct (Figure 4C). The analysis of the six most prevalent genera revealed significant differences in the respiratory microbiota of mice that exhibited varying symptoms post-influenza infection (Figure 4D). We hypothesise that the genus



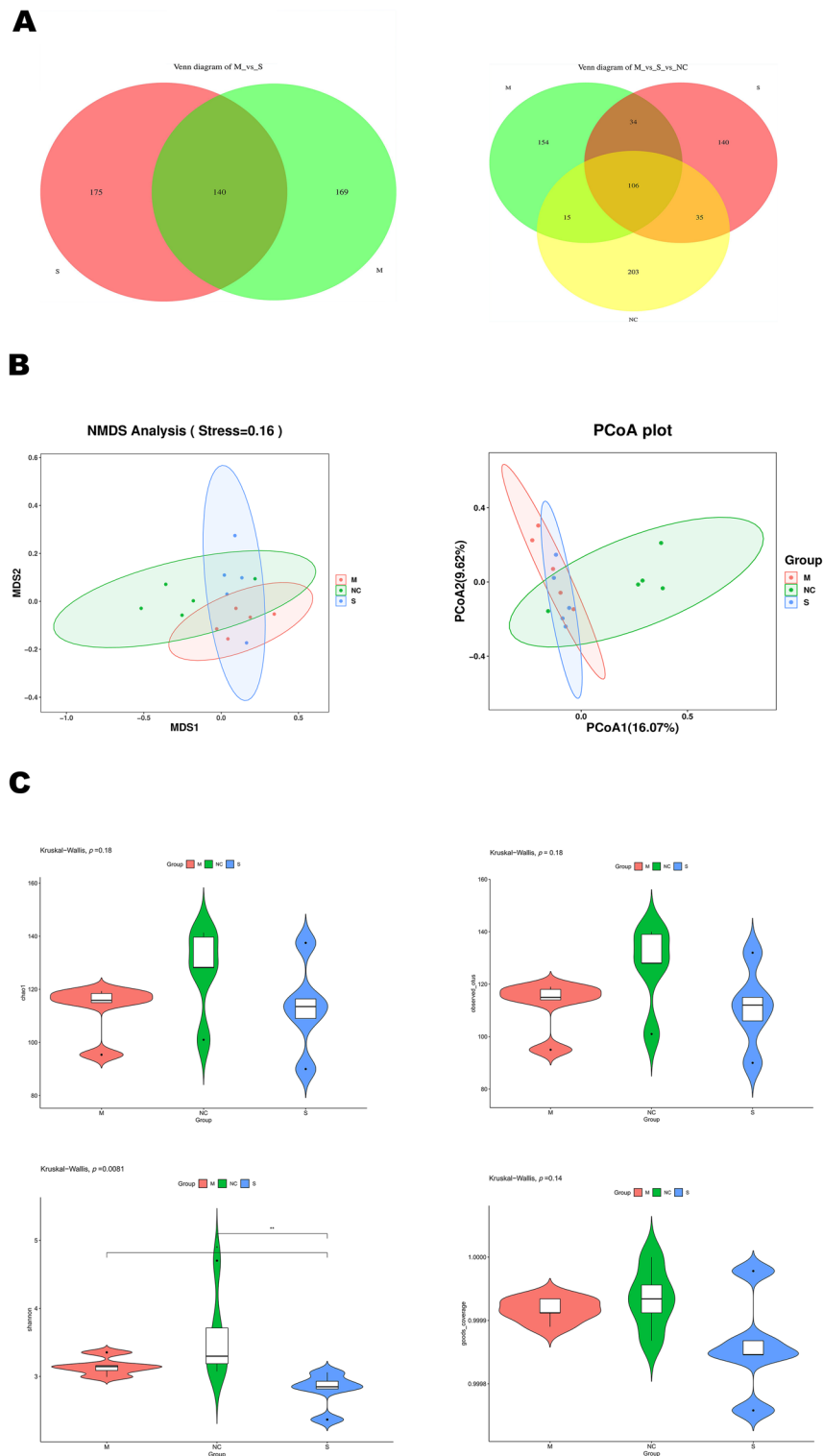


**Figure 3** Diversity of respiratory microbiota in mice analysed via alveolar lavage fluid. **A** Venn diagram showing shared and unique ASVs (species) derived from abundance tables. **B** PCoA and NMDS plots based on the Jaccard distance matrix for groups M and S. **C** Violin plots of subgroup differences analysed by Kruskal–Wallis test.

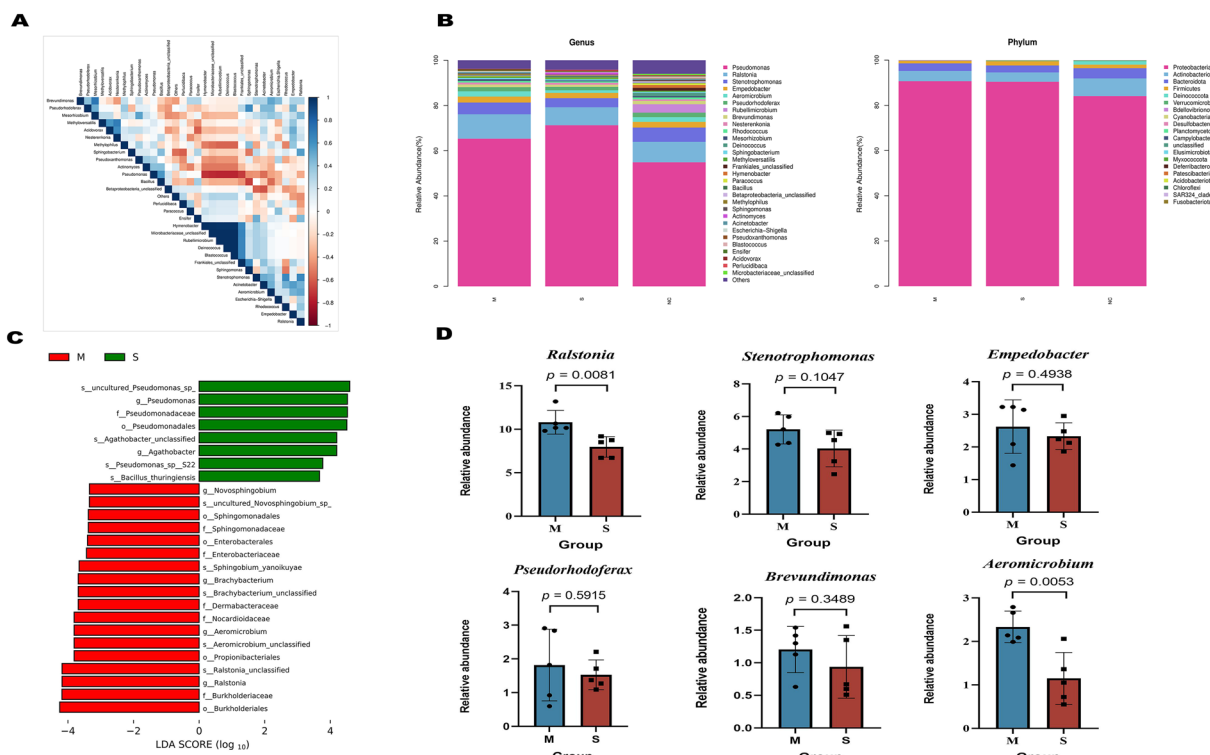


**Figure 4** Comparative analysis of microbial diversity in mouse respiratory systems. **A** Correlation heatmap (via Spearman's rank correlation) illustrating relationships among the top 30 microorganisms at the genus level, highlighting correlations and significance ( $P$ -value). **B** Relative abundance of bacterial phyla and genera across groups M, S, and NC. **C** LefSe analysis showing differences in species between groups M and S five days post-infection. **D**. Comparison of the six most abundant genera using Student's  $t$ -test.

*Aeromicrobium* may play a role in bolstering host defences against influenza.

***Aeromicrobium camelliae* is strongly associated with the viability of influenza-infected mice**

In this study, mice were subjected to an ATB solution to investigate the influence of *Aeromicrobium camelliae* on their resistance to influenza. Subsequently, *Aeromicrobium camelliae* was administered nasally prior to the infection (Figure 5A). Data suggested that *Aeromicrobium camelliae* markedly increased the survival rates of the recipient mice (Figure 5B and C). Control experiments, utilising ATB-prepped mice, were conducted to ascertain cytokine levels and scrutinise histological alterations and immunohistochemistry. On the fifth day post-infection, the bulk of the cytokines in *Aeromicrobium camelliae*-administered mice presented a significant surge in both groups (Figure 5F and H). Notably, cytokines TNF- $\alpha$ , IL-1 $\beta$ , and IL-6 registered lower levels in the serum and lungs of mice treated with *Aeromicrobium camelliae* than those treated with PBS. This outcome infers that *Aeromicrobium camelliae* might fortify the host against influenza by fine-tuning its immune mechanism. The results of the virus titre test showed

that the lung virus titre of the *Aeromicrobium camelliae* group was significantly lower than that of the PBS group (Figure 5D).

Furthermore, histological evaluations showed that on the fifth day after infection, the group that received PBS demonstrated significant pathological changes, including congestion, increased inflammatory cells, and a near-complete loss of alveolar structure. Conversely, those treated with *Aeromicrobium camelliae* demonstrated milder lung pathologies (Figure 5E). Immunohistochemical analyses further reinforced a decline in lung viral load for mice exhibiting a milder infection post *Aeromicrobium camelliae* administration (Figure 5G). This finding solidifies the proposition that *Aeromicrobium camelliae* potentially shields the host from influenza by modulating its immune response.

***Aeromicrobium* may protect hosts against influenza viruses by regulating respiratory microbial metabolism**

We conducted an analysis of respiratory microorganism metabolites using untargeted metabolomics techniques. The PCA plot reveals distinct variability in metabolic ions between the M and S groups (Figure 6C). The correlation heatmap indicates a significant positive correlation

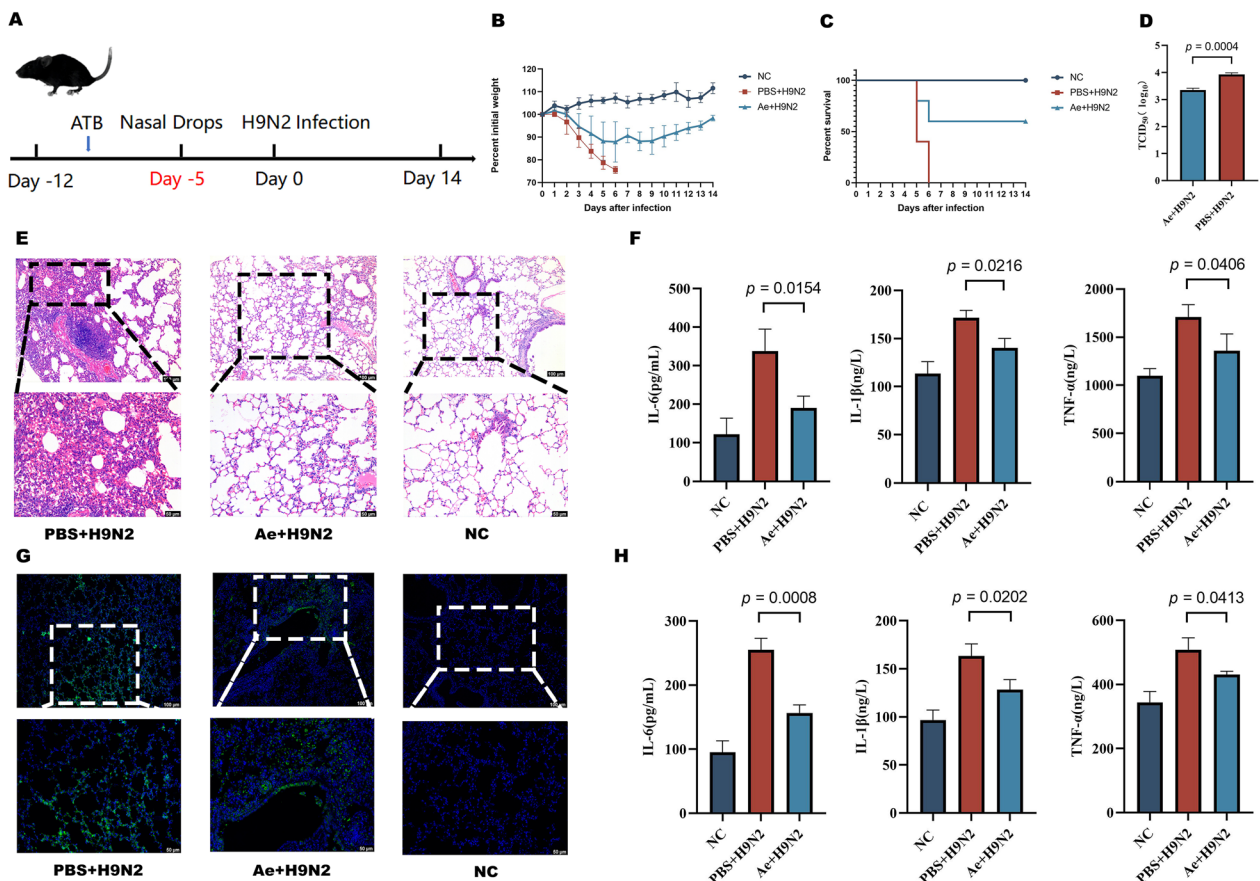


**Figure 5** The genus *Aeromicrobium* and its potential impact on diverse influenza responses in mice. **A** Experimental procedure. **B** Body weight variability. **C** Survival rates. **D** Pulmonary virus concentration ( $\log_{10}$ TCID<sub>50/g</sub> of lung tissue). **E** H&E staining of lung tissues. **F** Serum cytokine concentrations. **G** Immunohistochemical analysis of lungs. **H** Cytokine levels in lung tissues. Data are presented as mean  $\pm$  SD. PBS + H9N2: Control group; Ae + H9N2: Bacterial challenge group.

for LysoPE 16:0 (Figure 6B). Moreover, the differential ion histogram demonstrates the occurrence of both up-regulated and down-regulated differential ions in the M and S groups (Figure 6E). Metabolites such as LysoPE 16:0, LysoPG 16:0, LysoPC 16:1, LysoPC 16:0, and PG 34.1; PG (16:0/18:1) were identified (Figure 6D). These metabolites might contribute to the influenza resistance observed in the Donor M group of respiratory microorganisms. Upon integrating metabolomics and 16S in a multi-omics approach, differences between *Aeromicrobium* and LysoPE (16:0) emerged (Figure 6A). We hypothesise that *Aeromicrobium* may fortify hosts against influenza viruses through modulation of respiratory microbial metabolism.

**LysoPE protects hosts against influenza infection**

To ascertain whether LysoPE can defend against influenza infection in mice, LysoPE was administered, as previously mentioned, to ATB-treated mice through nasal drops. Subsequently, mice were inoculated

intranasally with the H9N2 virus (Figure 7A). As depicted in the graph, mice that received LysoPE exhibited enhanced survival rates and mitigated weight loss (Figure 7B and C). According to the virus titre test results, the lung virus titre of the LysoPE group was significantly lower than that of the Vehicle group (Figure 7D). In vivo, complementary animal studies were executed to investigate LysoPE’s anti-influenza mechanism more deeply. On the fifth day after infection, we collected samples of lung tissue, serum, and alveolar lavage fluid to measure cytokine levels, evaluate histological changes, and perform immunohistochemical assays. Notably, the concentrations of inflammatory cytokines TNF- $\alpha$ , IL-1 $\beta$ , and IL-6 were diminished in the serum and lungs of the LysoPE-treated mice on day five post-infection (Figure 7F and H). Histological evaluations coupled with immunohistochemical analyses further revealed that LysoPE treatment curtailed tissue damage and lessened the viral burden in the lungs (Figure 7E and G).

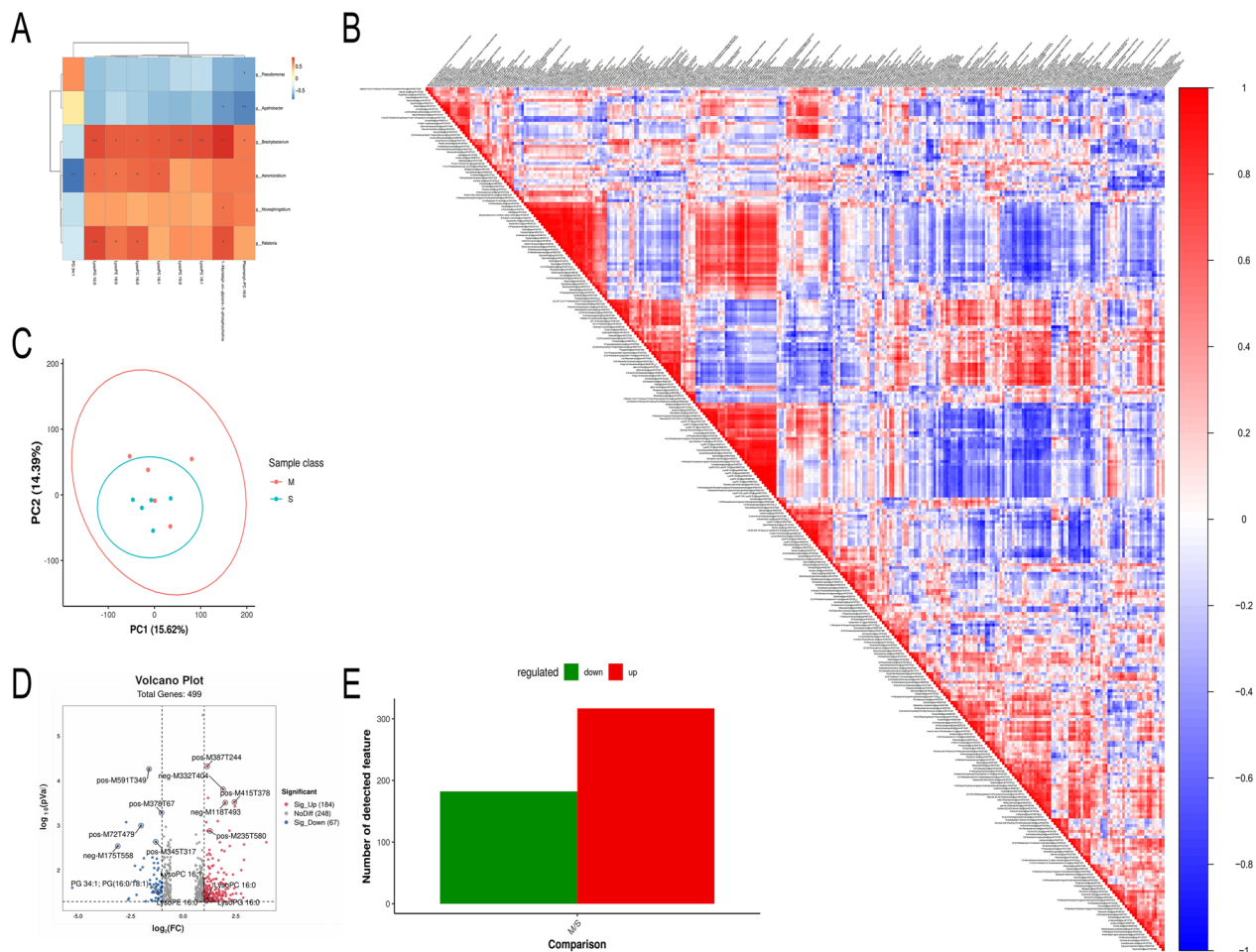


**Figure 6** Extensive metabolomic analysis of alveolar lavage fluid in mice. **A** Correlation graphs show associations between different genera and metabolites (via Spearman's correlation coefficient) integrating untargeted metabolomics with 16 s co-analysis. **B** Analysis of metabolites (post-normalisation) identified by ion profiles (red for positive correlations, blue for negative; the intensity of the colour indicates stronger correlation). **C** Principal Component Analysis (PCA) illustrates variability within and between groups. **D** Volcano plots, utilising differences in metabolic ions as the horizontal axis and  $-\log_{10}$  (q-value) as the vertical axis, aid in identifying significant metabolic variations. **E** Univariate analysis using fold-change and the t-test, enhanced by BH Correction for q-value and Variable Importance in Projection (VIP) scores from PLS-DA, identifies and highlights differentially expressed metabolic ions, culminating in a differential ion histogram.

Western blot analysis and qRT-PCR of isolated AMs showed decreased protein expression levels and transcription levels of INOS and COX-2 genes in LysoPE-treated mice compared with the Vehicle group (Figure 8A and B). As pivotal inflammatory mediators, INOS and COX-2 often serve as markers for gauging inflammation severity. This result underscores the potential of LysoPE to temper systemic inflammation, most likely through inhibiting INOS and COX-2 expression.

**Effect of LPS stimulation on transcript levels of cytokines associated with J774A.1 cells**

J774A.1 cells were exposed to varying concentrations (100, 500, 1000 ng/mL) of LPS for 6 h. Real-time

quantification results manifested that gene expression of inflammation-associated markers TNF- $\alpha$ , IL-1 $\beta$ , and IL-6 stimulated with 1ug/mL LPS was higher than that of the control group (Figure 9A).

**LysoPE inhibits LPS-induced expression of INOS and COX-2 in J774A.1 cells**

We employed qRT-PCR and protein blotting to assess the influence of LysoPE on INOS and COX-2 expression in J774A.1 cells. The results indicated that LPS treatment amplified mRNA expression of INOS and COX-2 in J774A.1 cells. However, when pre-treated with LysoPE, LPS-induced INOS and COX-2 expressions were significantly reduced (Figure 9B and C).

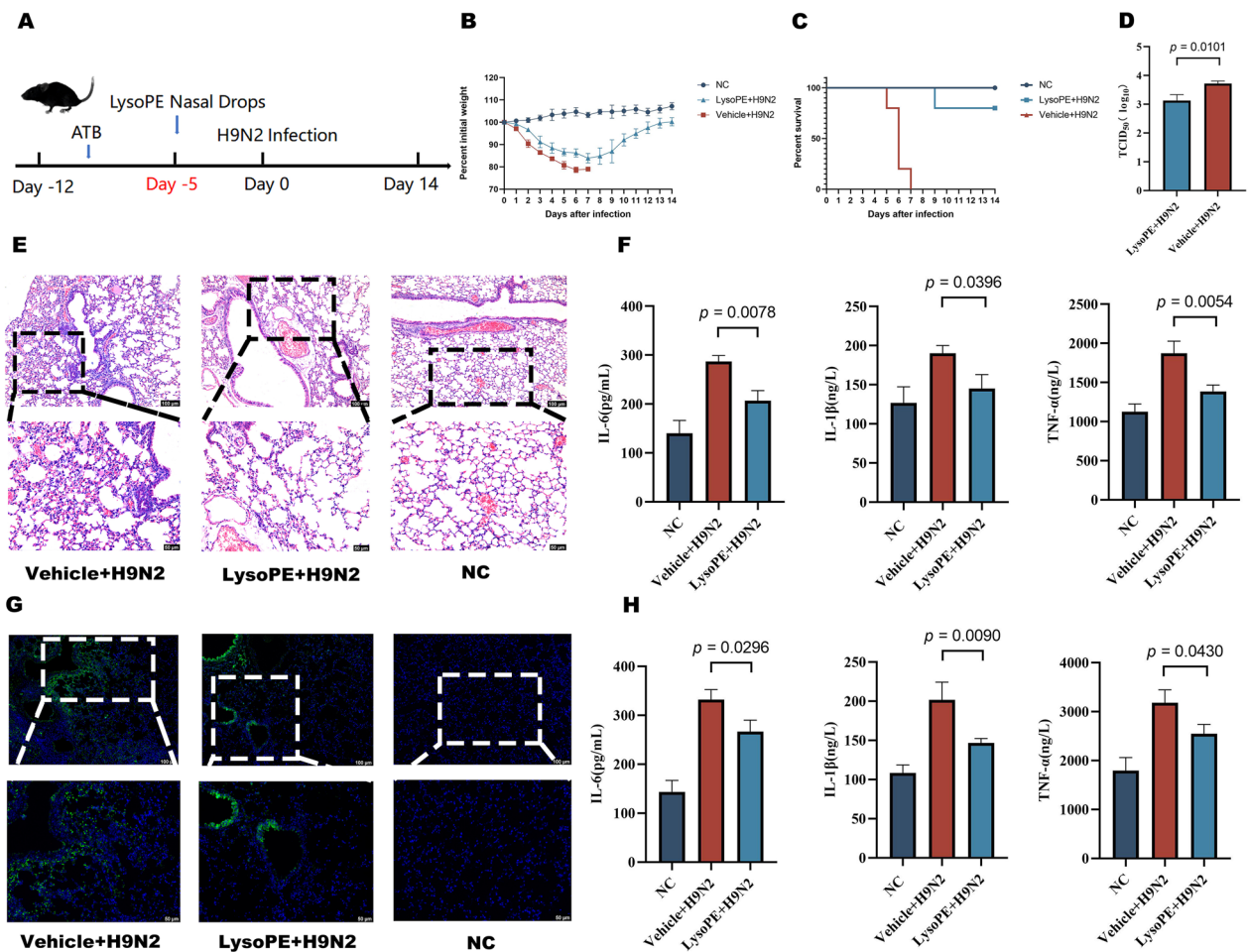


**Figure 7** Potential influence of the respiratory microbial metabolite LysoPE on heterogeneous influenza responses in mice. **A** Experimental procedure. **B** Variations in body weight. **C** Survival rate of mice. **D**. Viral load in lung tissue ( $\log_{10}$ TCID<sub>50</sub>/g). **E** H&E staining of lung tissues. **F** Serum cytokine levels. **G** Immunohistochemical analysis of lung tissues. **H**. Cytokine levels in lung tissues. Data are presented as mean  $\pm$  SD. Vehicle + H9N2: Control group; LysoPE + H9N2: Metabolite challenge group.

### Discussion

We present evidence that *Aeromicrobium camelliae* offers protective effects against the H9N2 influenza virus in mice. Furthermore, intranasal administration of LysoPE (16:0), a metabolite of respiratory microbiota, diminished the severity of influenza virus infections in mice.

Recent scientific research has increasingly emphasised the benefits of bacterial colonisation on mucosal surfaces across a range of fields, including nutrition, immunology, and behavioural studies. Historically, the lungs were presumed to be sterile environments. This presumption directed most research attention to the densely colonised gut microbiota. As such, limited data exist on the lung microbiota's role in regulating immunity and maintaining homeostasis in vivo [54–57]. Scientific methodologies have advanced significantly, particularly with the high-throughput sequencing of the 16S gene, which has greatly expanded our understanding of this field.

Moreover, recent studies employing advanced genomic technologies have highlighted the lungs' diverse microbial environment, which is essential for optimal lung health [58] and serves as a defensive barrier against respiratory diseases. The dynamic interplay among the lung microbiome, pathogenic viruses, and host immunity is pivotal in dictating lung inflammation and immune responses [59]. There is increasing evidence to suggest that the interaction between the microbiota in the lungs and the host's immune system is essential for maintaining a balanced immune system in the lungs.

Wang et al. reported that SPF mice were more vulnerable to acute inflammation and mortality post-influenza virus exposure compared to mice in natural environments [60]. Notably, the presence of commensal *S. aureus* significantly diminished influenza-mediated pulmonary immune damage, which is essential for resisting severe inflammatory responses. Zhang et al. leveraged LD<sub>50</sub> and

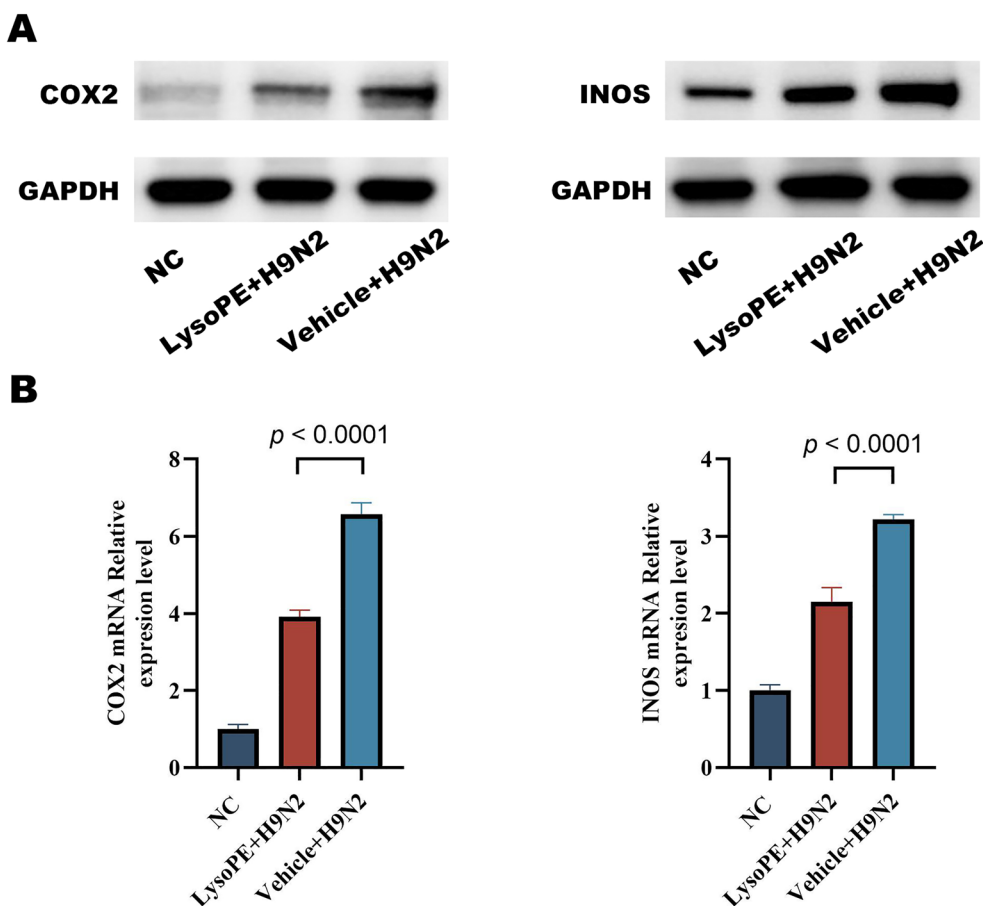


**Figure 8** Variability in influenza response in mice possibly due to respiratory microbial metabolite LysoPE. **A** Protein expression levels of INOS and COX-2 in alveolar macrophages. **B** mRNA transcription levels of INOS and COX-2 in alveolar macrophages. Data are expressed as mean  $\pm$  SD from three independent experiments.

macro-genome sequencing analysis to pinpoint specific anti-influenza gut microbes and decipher the underlying mechanisms [50]. They observed alterations in the mice’s gut microbiota post-influenza infection and dynamically mapped gut microbiota shifts.

Furthermore, the increased prevalence of deterioration-related bacteria, such as *Haemophilus*, *Pseudomonas*, and *Moraxella*, has been associated with conditions like cystic fibrosis (CF), chronic obstructive pulmonary disease (COPD), and other persistent lung diseases [61, 62]. Mathieu et al. documented an elevated presence of *Aspergillus* in asthmatic patients’ lung microbiota [63]. They found that discrepancies in the lung microbiota components were evident between lung cancer patients and healthy individuals. Typically, alpha diversity was considerably higher in non-tumour lung tissues compared to tumorous counterparts.

Laroumagne et al. identified gram-negative bacteria, including *Haemophilus influenzae*, *Enterobacter* spp, and *Escherichia coli*, colonising lung cancer patients’

respiratory tracts [64]. This finding suggests that certain pathogens might disrupt the respiratory microbiota balance, thereby modulating disease onset and progression. Similarly, our study devised an H9N2 infection mouse model, revealing varying clinical manifestations in mice post-H9N2 influenza virus infection. Respiratory microorganisms from the mild disease group exhibited a protective response against influenza, enhancing mouse survival rates.

We found that histological and immunohistochemical analyses corroborated that mice treated with respiratory microorganisms from the mild disease group exhibited fewer lung pathological alterations and a reduced viral load. Through 16 s sequencing, we distinguished pronounced differences in the respiratory microbiota between severely and mildly infected mice post-influenza. The *Proteobacteria*, *Actinobacteria*, *Bacteroidota*, *Firmicutes*, and *Deinococcota* were dominant in groups M and S. *Firmicutes* showed reduced abundance in Group M relative to Group S. Groups M

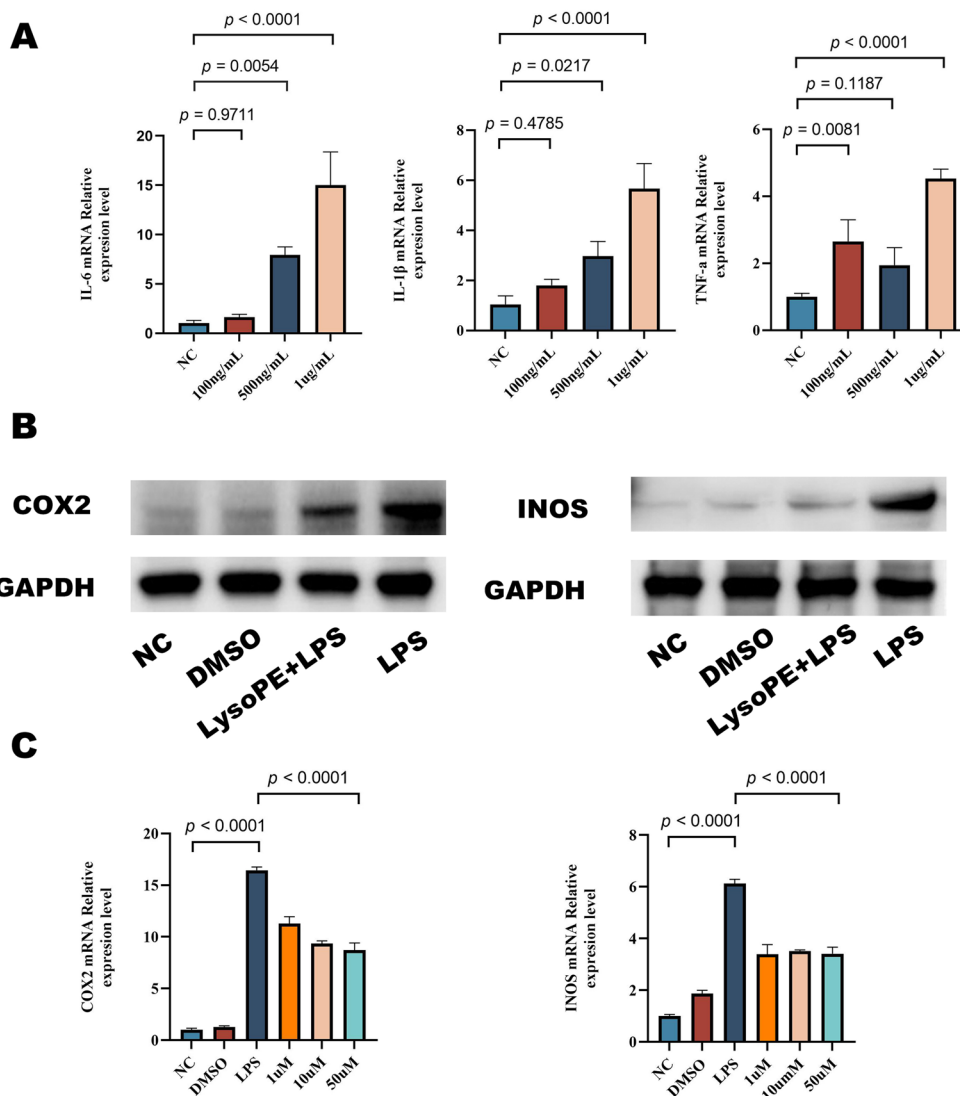


**Figure 9** LysoPE reduces LPS-induced expression of INOS and COX-2 in J774A.1 cells. **A** Gene expression of IL-6, TNF- $\alpha$ , IL-1 $\beta$  in J774A.1 cells post-exposure to various LPS concentrations for 6 h. **B** Protein expression levels of INOS and COX-2 after 24 h exposure to LPS following 50  $\mu$ M LysoPE pretreatment. **C** mRNA transcription levels of INOS and COX-2 in LPS-stimulated cells after 24 h pretreatment with 50  $\mu$ M LysoPE. Data are presented as mean  $\pm$  SD from three independent experiments.

and S were dominated by *Pseudomonas* spp., *Ralstonia* spp., *Stenotrophomonas* spp., *Empedobacter* spp., and *Aeromicrobium* spp.

*Pseudomonas* spp. were more abundant in group S than group M, whereas *Ralstonia* spp., *Stenotrophomonas* spp., *Empedobacter* spp., and *Aeromicrobium* spp. were more prevalent in group M. Marked differences between groups M and S were also observed for *Pseudomonas* spp., *Ralstonia* spp., and *Aeromicrobium* spp. Such variances in respiratory microorganisms between groups post-influenza infection might contribute to the diverse clinical manifestations following influenza infection.

Recent research on the lung microbiome has improved our understanding of the potential therapeutic targets found within commensal flora for an array of respiratory ailments [65]. Probiotics have gained widespread acceptance in treating infectious respiratory diseases due to their pronounced effects in bolstering the host's immunity and countering pathogenic invasions [66]. Numerous studies confirm that introducing oral or nasal lactobacilli and various probiotics can recalibrate the respiratory tract's innate immune response, thus bolstering resistance against influenza viruses. Additionally, several strains of *lactobacilli* (LAB) are known for invigorating

the mucosal immune system and offering robust defence against *Streptococcus pneumoniae* infections [67–69]. Zhang et al. and Shida et al. established that probiotic blends, such as Clear Run yoghurt and *Lactobacillus casei*, fortify the respiratory tract. Their research particularly emphasised a reduction of infection occurrences, diminished duration, lessened severity, and, notably, enhanced immune markers [70, 71].

Furthermore, infant formula fortified with prebiotics and probiotics has effectively curtailed respiratory infections [72]. Tomita et al.'s animal study on RSV infection clarified that intranasal delivery of *Lactobacillus rhamnosus* heightened mice resistance to RSV exposure [73]. Our current research indicated that the mice treated with *Aeromicrobium camelliae* exhibited substantial resistance to severe influenza virus infections, which is evident through limited weight loss, diminished lung viral loads, and increased survival rates. Consequently, *Aeromicrobium camelliae* exhibits potential anti-influenza properties, marking it as a promising probiotic strain.

As we have shown, microbial byproducts are pivotal in shaping host health and specific disease manifestations [74]. For instance, gut-derived metabolites, such as succinate and itaconic acid, influence macrophage phagocytic activity and aid in the clearance of bacterial infection [75]. Steed et al. demonstrated that the inclusion of desamino-tyrosine (DAT, a flavonoid degradation derivative of intestinal bacteria) in drinking water shielded mice from the repercussions of influenza virus infections, particularly mortality and weight reductions [76]. In a separate investigation, Wypych et al. identified that cresyl sulfate (PCS), a culmination of L-tyrosine metabolism facilitated by the gut microbiota, safeguards mice from allergic respiratory inflammation [77]. Such revelations highlight the indispensable role of microbiota-synthesised metabolites in maintaining organismal health. Similarly, our analysis showed that mice administered with nasal drops of LysoPE showcased heightened resilience against the influenza virus.

Moreover, histopathological and immunohistochemical assessments revealed minimal pathological deviations and reduced lung viral concentrations, thus enhancing survival prospects. Utaipan T emphasised the efficacy of ursodeoxycholanoyl lysophosphatidyl ethanolamide in averting CD95 / FAS-induced fulminant hepatitis [78]. We suggest that certain compounds, specifically LysoPE, possess anti-inflammatory properties. However, further research is needed to understand the anti-inflammatory mechanism of LysoPE (16:0) fully.

In conclusion, we observed heterogeneity in the response to influenza infection in a mouse model. Moreover, we identified *Aeromicrobium* as a member of the respiratory microbiota that can protect against influenza

infection. We demonstrate that the genus *Aeromicrobium* is elevated in abundance in the lungs following influenza virus infection, thereby protecting the host against the virus. Our study also represents a new way in which the respiratory microbiota can protect the host against infection, possibly through a novel interaction between the host and the respiratory microbiota. In addition to the gut microbiota, we also found that respiratory microbiota can be used as a novel biomarker to predict the severity and mortality of influenza patients, which may help provide a new idea for the precise treatment of influenza in the future.

#### Acknowledgements

This work was supported by the National Natural Science Foundation of China (U21A20261, 32202819, 31941018, 31972696 and 32072888), the China Agriculture Research System of MOF and MARA (CARS-35), the Science and Technology Development Programme of Jilin Province (20190301042NY, YDZJ202102CXJD029, and 20210202102NC).

#### Authors' contributions

CW and GY designed the experiments. QY wrote the paper. BZ and HH organised and typeset the images. TN, WY, MS, RZ, and JX helped with sample collection and data presentation. MS, BZ, and JX performed the majority of the experiments and analysed the data. BZ, JX, TY, MS, YW, and CS helped revise the manuscript. CW and GY supervised the study. JX drafted the original paper. All authors read and approved the final manuscript.

#### Declarations

##### Competing interests

The authors declare that they have no competing interests.

Received: 8 April 2024 Accepted: 13 August 2024

Published online: 11 October 2024

#### References

1. Wu NC, Wilson IA (2020) Influenza hemagglutinin structures and antibody recognition. *Cold Spring Harb Perspect Med* 10:a038778
2. Eladl AH, Mosad SM, El-Shafei RA, Saleh RM, Ali HS, Badawy BM, Elshal MF (2020) Immunostimulant effect of a mixed herbal extract on infectious bursal disease virus (IBDV) vaccinated chickens in the context of a co-infection model of avian influenza virus H9N2 and IBDV. *Comp Immunol Microbiol Infect Dis* 72:101505
3. Dong J, Zhou Y, Pu J, Liu L (2022) Status and challenges for vaccination against avian H9N2 influenza virus in China. *Life (Basel)* 12:1326
4. Diefenbacher M, Tan TJC, Bauer DLV, Stadtmueller BM, Wu NC, Brooke CB (2022) Interactions between influenza A virus nucleoprotein and gene segment untranslated regions facilitate selective modulation of viral gene expression. *J Virol* 96:e0020522
5. Verhagen JH, Lexmond P, Vuong O, Schutten M, Guldemeester J, Osterhaus AD, Elbers AR, Slaterus R, Hornman M, Koch G, Fouchier RA (2017) Discordant detection of avian influenza virus subtypes in time and space between poultry and wild birds; towards improvement of surveillance programs. *PLoS One* 12:e0173470
6. Yan W, Cui H, Engelsma M, Beerens N, van Oers MM, de Jong MCM, Li X, Liu Q, Yang J, Teng Q, Li Z (2022) Molecular and antigenic characterization of avian H9N2 viruses in Southern China. *Microbiol Spectr* 10:e0082221
7. Sagong M, Lee KN, Lee EK, Kang H, Choi YK, Lee YJ (2023) Current situation and control strategies of H9N2 avian influenza in South Korea. *J Vet Sci* 24:e5



8. Homme PJ, Easterday BC (1970) Avian influenza virus infections. I. Characteristics of influenza A-turkey-Wisconsin-1966 virus. *Avian Dis* 14:66–74
9. Fallah Mehrabadi MH, Motamed N, Ghalyanchilangeroudi A, Tehrani F, Borhani Kia A (2020) Avian influenza (H9N2 subtype) in Iranian broiler farms: a cross-sectional study. *Arch Razi Inst* 75:359–366
10. Awuni JA, Bianco A, Dogbey OJ, Fusaro A, Yingar DT, Salviato A, Ababio PT, Milani A, Bonfante F, Monne I (2019) Avian influenza H9N2 subtype in Ghana: virus characterization and evidence of co-infection. *Avian Pathol* 48:470–476
11. Peiris M, Yuen KY, Leung CW, Chan KH, Ip PL, Lai RW, Orr WK, Shortridge KF (1999) Human infection with influenza H9N2. *Lancet* 354:916–917
12. Arai Y, Elgandy EM, Daidoji T, Ibrahim MS, Ono T, Sriwilaijaroen N, Suzuki Y, Nakaya T, Matsumoto K, Watanabe Y (2020) H9N2 influenza virus infections in human cells require a balance between neuraminidase sialidase activity and hemagglutinin receptor affinity. *J Virol* 94:e01210-20
13. Peacock THP, James J, Sealy JE, Iqbal M (2019) A global perspective on H9N2 avian influenza virus. *Viruses* 11:620
14. Wang S, Jiang N, Shi W, Yin H, Chi X, Xie Y, Hu J, Zhang Y, Li H, Chen JL (2021) Co-infection of H9N2 influenza A virus and *Escherichia coli* in a BALB/c mouse model aggravates lung injury by synergistic effects. *Front Microbiol* 12:670688
15. Kong L, You R, Zhang D, Yuan Q, Xiang B, Liang J, Lin Q, Ding C, Liao M, Chen L, Ren T (2021) Infectious bronchitis virus infection increases pathogenicity of H9N2 avian influenza virus by inducing severe inflammatory response. *Front Vet Sci* 8:824179
16. Hassan KE, Ali A, Shany SAS, El-Kady MF (2017) Experimental co-infection of infectious bronchitis and low pathogenic avian influenza H9N2 viruses in commercial broiler chickens. *Res Vet Sci* 115:356–362
17. Arafat N, Eladl AH, Marghani BH, Saif MA, El-Shafei RA (2018) Enhanced infection of avian influenza virus H9N2 with infectious laryngeotracheitis vaccination in chickens. *Vet Microbiol* 219:8–16
18. Sun W, Cheng SSM, Lam KNT, Kwan TC, Wong RWK, Lau LHK, Liu GYZ, Luk LLH, Li JKC, Gu H, Peiris M, Poon LLM (2022) Natural reassortment of Eurasian avian-like swine H1N1 and avian H9N2 influenza viruses in pigs, China. *Emerg Infect Dis* 28:1509–1512
19. Pu J, Yin Y, Liu J, Wang X, Zhou Y, Wang Z, Sun Y, Sun H, Li F, Song J, Qu R, Gao W, Wang D, Wang Z, Yan S, Chen M, Zeng J, Jiang Z, Sun H, Zong Y, Wang C, Tong Q, Bi Y, Huang Y, Du X, Chang KC, Liu J (2021) Reassortment with dominant chicken H9N2 influenza virus contributed to the fifth H7N9 virus human epidemic. *J Virol* 95:e01578
20. Arai Y, Ibrahim MS, Elgandy EM, Daidoji T, Ono T, Suzuki Y, Nakaya T, Matsumoto K, Watanabe Y (2019) Genetic compatibility of reassortants between avian H5N1 and H9N2 influenza viruses with higher pathogenicity in mammals. *J Virol* 93:e01969
21. Sun Y, Liu J (2015) H9N2 influenza virus in China: a cause of concern. *Protein Cell* 6:18–25
22. Song W, Qin K (2020) Human-infecting influenza A (H9N2) virus: a forgotten potential pandemic strain? *Zoonoses Public Health* 67:203–212
23. Poretsky R, Rodriguez RL, Luo C, Tsementzi D, Konstantinidis KT (2014) Strengths and limitations of 16S rRNA gene amplicon sequencing in revealing temporal microbial community dynamics. *PLoS One* 9:e93827
24. Mizrahi-Man O, Davenport ER, Gilad Y (2013) Taxonomic classification of bacterial 16S rRNA genes using short sequencing reads: evaluation of effective study designs. *PLoS One* 8:e53608
25. Martín R, Langella P (2019) Emerging health concepts in the probiotics field: streamlining the definitions. *Front Microbiol* 10:1047
26. Zhou B, Albarracín L, Indo Y, Arce L, Masumizu Y, Tomokiyo M, Islam MA, García-Castillo V, Ikeda-Ohtsubo W, Nochi T, Morita H, Takahashi H, Kurata S, Villena J, Kitazawa H (2020) Selection of immunobiotic *Ligilactobacillus salivarius* strains from the intestinal tract of wakame-fed pigs: functional and genomic studies. *Microorganisms* 8:1659
27. Luo X, Kong Q, Wang Y, Duan X, Wang P, Li C, Huan Y (2021) Colonization of *Clostridium butyricum* in rats and its effect on intestinal microbial composition. *Microorganisms* 9:1573
28. Bian X, Wu W, Yang L, Lv L, Wang Q, Li Y, Ye J, Fang D, Wu J, Jiang X, Shi D, Li L (2019) Administration of *Akkermansia muciniphila* ameliorates dextran sulfate sodium-induced ulcerative colitis in mice. *Front Microbiol* 10:2259
29. Huffnagle GB, Dickson RP, Lukacs NW (2017) The respiratory tract microbiome and lung inflammation: a two-way street. *Mucosal Immunol* 10:299–306
30. Piccioni A, Franza L, Vaccaro V, Saviano A, Zanza C, Candelli M, Covino M, Franceschi F, Ojetti V (2021) Microbiota and probiotics: the role of *Limosilactobacillus Reuteri* in diverticulitis. *Medicina (Kaunas)* 57:802
31. Pascale A, Marchesi N, Marelli C, Coppola A, Luzi L, Govoni S, Giustina A, Gazzaruso C (2018) Microbiota and metabolic diseases. *Endocrine* 61:357–371
32. Man WH, de Steenhuijsen Pijters WA, Bogaert D (2017) The microbiota of the respiratory tract: gatekeeper to respiratory health. *Nat Rev Microbiol* 15:259–270
33. Hoggard M, Waldvogel-Thurlow S, Zoing M, Chang K, Radcliff FJ, Wagner Mackenzie B, Biswas K, Douglas RG, Taylor MW (2018) Inflammatory endotypes and microbial associations in chronic rhinosinusitis. *Front Immunol* 9:2065
34. Ortiz Moyano R, Raya Tonetti F, Tomokiyo M, Kanmani P, Vizoso-Pinto MG, Kim H, Quilodrán-Vega S, Melnikov V, Alvarez S, Takahashi H, Kurata S, Kitazawa H, Villena J (2020) The ability of respiratory commensal bacteria to beneficially modulate the lung innate immune response is a strain dependent characteristic. *Microorganisms* 8:727
35. Chun C, Zheng L, Colgan SP (2017) Tissue metabolism and host-microbial interactions in the intestinal mucosa. *Free Radic Biol Med* 105:86–92
36. Sittipo P, Shim JW, Lee YK (2019) Microbial metabolites determine host health and the status of some diseases. *Int J Mol Sci* 20:5296
37. Ramírez-Pérez O, Cruz-Ramón V, Chinchilla-López P, Méndez-Sánchez N (2017) The role of the gut microbiota in bile acid metabolism. *Ann Hepatol* 16:s15–s20
38. He J, Zhang P, Shen L, Niu L, Tan Y, Chen L, Zhao Y, Bai L, Hao X, Li X, Zhang S, Zhu L (2020) Short-chain fatty acids and their association with signaling pathways in inflammation, glucose and lipid metabolism. *Int J Mol Sci* 21:6356
39. Hu B, Elinav E, Huber S, Strowig T, Hao L, Hafemann A, Jin C, Wunderlich C, Wunderlich T, Eisenbarth SC, Flavell RA (2013) Microbiota-induced activation of epithelial IL-6 signaling links inflammasome-driven inflammation with transmissible cancer. *Proc Natl Acad Sci U S A* 110:9862–9867
40. Hsiao EY, McBride SW, Hsien S, Sharon G, Hyde ER, McCue T, Codelli JA, Chow J, Reisman SE, Petrosino JF, Patterson PH, Mazmanian SK (2013) Microbiota modulate behavioral and physiological abnormalities associated with neurodevelopmental disorders. *Cell* 155:1451–1463
41. Ma Y, Han X, Fang J, Jiang H (2022) Role of dietary amino acids and microbial metabolites in the regulation of pig intestinal health. *Anim Nutr* 9:1–6
42. Levy M, Thaiss CA, Elinav E (2016) Metabolites: messengers between the microbiota and the immune system. *Genes Dev* 30:1589–1597
43. Đukanović N, Obradović S, Zdravković M, Đurašević S, Stojković M, Tosti T, Jasnić N, Đorđević J, Todorović Z (2021) Lipids and antiplatelet therapy: important considerations and future perspectives. *Int J Mol Sci* 22:3180
44. Yamamoto Y, Sakurai T, Chen Z, Inoue N, Chiba H, Hui SP (2022) Lysophosphatidylethanolamine affects lipid accumulation and metabolism in a human liver-derived cell line. *Nutrients* 14:579
45. Nishina A, Kimura H, Sekiguchi A, Fukumoto RH, Nakajima S, Furukawa S (2006) Lysophosphatidylethanolamine in *Griifola frondosa* as a neurotrophic activator via activation of MAPK. *J Lipid Res* 47:1434–1443
46. Park SJ, Im DS (2021) 2-Arachidonyl-lysophosphatidylethanolamine induces anti-inflammatory effects on macrophages and in carrageenan-induced paw edema. *Int J Mol Sci* 22:4865
47. Hisano K, Yoshida H, Kawase S, Mimura T, Haniu H, Tsukahara T, Kurihara T, Matsuda Y, Saito N, Uemura T (2021) Abundant oleoyl-lysophosphatidylethanolamine in brain stimulates neurite outgrowth and protects against glutamate toxicity in cultured cortical neurons. *J Biochem* 170:327–336
48. Hisano K, Kawase S, Mimura T, Yoshida H, Yamada H, Haniu H, Tsukahara T, Kurihara T, Matsuda Y, Saito N, Uemura T (2021) Structurally different lysophosphatidylethanolamine species stimulate neurite outgrowth in cultured cortical neurons via distinct G-protein-coupled receptors and signaling cascades. *Biochem Biophys Res Commun* 534:179–185
49. Xing JH, Shi CW, Sun MJ, Gu W, Zhang RR, Chen HL, Li Y, Wang D, Li J, Niu TM, Huang QT, Qian JH, Huang HB, Jiang YL, Wang JZ, Cao X, Wang N, Zeng Y, Yang GL, Yang WT, Wang CF (2022) *Lactiplantibacillus plantarum* 0111 protects against influenza virus by modulating intestinal microbial-mediated immune responses. *Front Microbiol* 13:820484
50. Zhang Q, Hu J, Feng JW, Hu XT, Wang T, Gong WX, Huang K, Guo YX, Zou Z, Lin X, Zhou R, Yuan YQ, Zhang AD, Wei H, Cao G, Liu C, Chen LL, Jin ML (2020) Influenza infection elicits an expansion of gut population of

- endogenous *Bifidobacterium animalis* which protects mice against infection. *Genome Biol* 21:99
51. Zhang S, Zhu L, Dai H, Pan L (2021) Silencing ROCK1 ameliorates ventilator-induced lung injury in mice by inhibiting macrophages' NLRP3 signaling. *Int Immunopharmacol* 101:108208
  52. Yang D, Chen X, Wang J, Lou Q, Lou Y, Li L, Wang H, Chen J, Wu M, Song X, Qian Y (2019) Dysregulated lung commensal bacteria drive interleukin-17B production to promote pulmonary fibrosis through their outer membrane vesicles. *Immunity* 50:692–706
  53. Reed LJ, Muench H (1938) A simple method of estimating fifty per cent endpoints. *Am J Epidemiol* 27:493–497
  54. Relman DA (2012) Microbiology: learning about who we are. *Nature* 486:194–195
  55. O'Dwyer DN, Dickson RP, Moore BB (2016) The lung microbiome, immunity, and the pathogenesis of chronic lung disease. *J Immunol* 196:4839–4847
  56. Consortium HMP (2012) A framework for human microbiome research. *Nature* 486:215–221
  57. Consortium HMP (2012) Structure, function and diversity of the healthy human microbiome. *Nature* 486:207–214
  58. Hilty M, Burke C, Pedro H, Cardenas P, Bush A, Bossley C, Davies J, Ervine A, Poulter L, Pachter L, Moffatt MF, Cookson WO (2010) Disordered microbial communities in asthmatic airways. *PLoS One* 5:e8578
  59. Clark SE (2020) Commensal bacteria in the upper respiratory tract regulate susceptibility to infection. *Curr Opin Immunol* 66:42–49
  60. Wang J, Li F, Sun R, Gao X, Wei H, Li LJ, Tian Z (2013) Bacterial colonization dampens influenza-mediated acute lung injury via induction of M2 alveolar macrophages. *Nat Commun* 4:2106
  61. Millares L, Ferrari R, Gallego M, Garcia-Nuñez M, Pérez-Brocal V, Espasa M, Pomares X, Monton C, Moya A, Monsó E (2014) Bronchial microbiome of severe COPD patients colonised by *Pseudomonas aeruginosa*. *Eur J Clin Microbiol Infect Dis* 33:1101–1111
  62. Dickson RP, Erb-Downward JR, Huffnagle GB (2013) The role of the bacterial microbiome in lung disease. *Expert Rev Respir Med* 7:245–257
  63. Mathieu E, Escribano-Vazquez U, Descamps D, Cherbuy C, Langella P, Riffault S, Remot A, Thomas M (2018) Paradigms of lung microbiota functions in health and disease, particularly, in asthma. *Front Physiol* 9:1168
  64. Laroumagne S, Lepage B, Hermant C, Plat G, Phelippeau M, Bigay-Game L, Lozano S, Guibert N, Segonds C, Mallard V, Augustin N, Didier A, Mazieres J (2013) Bronchial colonisation in patients with lung cancer: a prospective study. *Eur Respir J* 42:220–229
  65. Li Z, Li Y, Sun Q, Wei J, Li B, Qiu Y, Liu K, Shao D, Ma Z (2022) Targeting the pulmonary microbiota to fight against respiratory diseases. *Cells* 11:916
  66. Debnath N, Kumar A, Yadav AK (2022) Probiotics as a biotherapeutics for the management and prevention of respiratory tract diseases. *Microbiol Immunol* 66:277–291
  67. Villena J, Oliveira ML, Ferreira PC, Salva S, Alvarez S (2011) Lactic acid bacteria in the prevention of pneumococcal respiratory infection: future opportunities and challenges. *Int Immunopharmacol* 11:1633–1645
  68. Tonetti FR, Islam MA, Vizoso-Pinto MG, Takahashi H, Kitazawa H, Villena J (2020) Nasal priming with immunobiotic lactobacilli improves the adaptive immune response against influenza virus. *Int Immunopharmacol* 78:106115
  69. Lehtoranta L, Pitkäranta A, Korpela R (2014) Probiotics in respiratory virus infections. *Eur J Clin Microbiol Infect Dis* 33:1289–1302
  70. Zhang H, Miao J, Su M, Liu BY, Liu Z (2021) Effect of fermented milk on upper respiratory tract infection in adults who lived in the haze area of Northern China: a randomized clinical trial. *Pharm Biol* 59:647–652
  71. Shida K, Sato T, Iizuka R, Hoshi R, Watanabe O, Igarashi T, Miyazaki K, Nanno M, Ishikawa F (2017) Daily intake of fermented milk with *Lactobacillus casei* strain Shirota reduces the incidence and duration of upper respiratory tract infections in healthy middle-aged office workers. *Eur J Nutr* 56:45–53
  72. Rashidi K, Darand M, Garousi N, Dehghani A, Alizadeh S (2021) Effect of infant formula supplemented with prebiotics and probiotics on incidence of respiratory tract infections: a systematic review and meta-analysis of randomized clinical trials. *Complement Ther Med* 63:102795
  73. Tomosada Y, Chiba E, Zelaya H, Takahashi T, Tsukida K, Kitazawa H, Alvarez S, Villena J (2013) Nasally administered *Lactobacillus rhamnosus* strains differentially modulate respiratory antiviral immune responses and induce protection against respiratory syncytial virus infection. *BMC Immunol* 14:40
  74. Postler TS, Ghosh S (2017) Understanding the holobiont: how microbial metabolites affect human health and shape the immune system. *Cell Metab* 26:110–130
  75. O'Callaghan AA, Dempsey E, Iyer N, Stiegeler S, Mercurio K, Corr SC (2021) Intestinal metabolites influence macrophage phagocytosis and clearance of bacterial infection. *Front Cell Infect Microbiol* 11:622491
  76. Steed AL, Christophi GP, Kaiko GE, Sun L, Goodwin VM, Jain U, Esaulova E, Artyomov MN, Morales DJ, Holtzman MJ, Boon ACM, Lenschow DJ, Stapenbeck TS (2017) The microbial metabolite desaminotyrosine protects from influenza through type I interferon. *Science* 357:498–502
  77. Wypych TP, Pattaroni C, Perdijk O, Yap C, Trompette A, Anderson D, Creek DJ, Harris NL, Marsland BJ (2021) Microbial metabolism of L-tyrosine protects against allergic airway inflammation. *Nat Immunol* 22:279–286
  78. Utaipan T, Otto AC, Gan-Schreier H, Chunglok W, Pathil A, Stremmel W, Chamulitrat W (2017) Ursodeoxycholy l lysophosphatidylethanolamide protects against CD95/FAS-induced fulminant hepatitis. *Shock* 48:251–259

## Publisher's Note

Springer Nature remains neutral with regard to jurisdictional claims in published maps and institutional affiliations.